The Astrophysical Journal Letters, 873:L2 (8pp), 2019 March 1 https://doi.org/10.3847/2041-8213/ab06cb


# Anchor Point of Electron Acceleration around Dipolarization Fronts in Space Plasmas

C. M. Liu and H. S. Fu
School of Space and Environment, Beihang University, Beijing, People's Republic of China; huishanf@gmail.com
*Received 2018 December 15; revised 2019 February 3; accepted 2019 February 13; published 2019 February 27*

## Abstract

An anchor point, which is an energy threshold above which electrons are accelerated and below which electrons are decelerated, has recently been reported within the dipolarizing flux bundles behind dipolarization fronts (DFs) both in observations and simulations. However, what determines this point and how it is formed remain unclear. In this study, we investigate for the first time the formation of this point and the relation between this point and the plasma properties by considering a large amount of DF events measured by Cluster. We find a good correlation between this anchor point and the plasma-sheet density and temperature. We notice that such a point appears primarily in the DF events associated with strong whistlers, suggesting that it is formed due to wave-particle interactions near DFs. Quantitatively, we establish a model for the anchor point, $E_{\rm AP} = 10^{2.2\pm0.3} \times (N/T)^{-0.6\pm0.1}$ eV, where $N$ and $T$ are the normalized plasma-sheet density and temperature, respectively. With this model, we can predict the electron acceleration features behind DFs, by monitoring plasma properties in the plasma sheet. Such a model can be crucial for understanding electron acceleration regions elsewhere in space, such as reconnection diffusion region and collisionless shocks.

*Key words:* acceleration of particles – magnetic reconnection

## 1. Introduction

A dipolarization front (DF), which is an earthward-propagating magnetic structure with a scale of ion inertial length (Khotyaintsev et al. 2011; Fu et al. 2012a), is characterized by the dramatic increase of the $Z$-component (in the Geocentric Solar Magnetospheric (GSM) coordinates) of magnetic field (e.g., Nakamura et al. 2002; Runov et al. 2009; Sergeev et al. 2009; Zhou et al. 2009; Fu et al. 2012b; Liu et al. 2013) and is frequently preceded by a $B_z$ dip (e.g., Yao et al. 2015). It is usually embedded in the high-speed plasma jets or bursty bulk flows in the magnetotail (e.g., Cao et al. 2006, 2008, 2013; Pritchett & Runov 2017), separating hot tenuous plasmas from ambient cold dense plasmas. The transient reconnection in the midtail has been suggested as a possible mechanism responsible for the formation of DFs in both simulations (e.g., Sitnov et al. 2009) and observations (e.g., Fu et al. 2013a; Xu et al. 2018a).

After its formation inside the reconnection diffusion region in the midtail, a DF can propagate toward the Earth over a long distance more than 10 $R_E$ (Runov et al. 2009), with a coherent shape that is convex in the equatorial plane when viewed from the Earth (e.g., Liu et al. 2013). During the DF's earthward propagation, electrons are usually accelerated up to suprathermal energies inside the flux pileup regions (FPRs; e.g., Khotyaintsev et al. 2011) or dipolarizing flux bundles (DFBs; e.g., Liu et al. 2013) behind the DF. These electrons are either energized by adiabatic processes (e.g., Ashour-Abdalla et al. 2011; Fu et al. 2011, 2013b; Gabrielse et al. 2012; Pan et al. 2012; Birn et al. 2013; Wu et al. 2013; Zhou et al. 2013; Duan et al. 2014; Huang et al. 2015b; Lu et al. 2016; Liu et al. 2017a, 2017b, 2017c, 2018d; Xu et al. 2018b) or accelerated by non-adiabatic processes (e.g., Zhou et al. 2009; Deng et al. 2010; Khotyaintsev et al. 2011; Huang et al. 2012; Fu et al. 2014a, 2014b; Hwang et al. 2014; Yang et al. 2017). The adiabatic process, including Fermi and betatron acceleration (Fu et al. 2011; Wu et al. 2013; Liu et al. 2017b), can uniformly raise electron energy without changing the power-law index in the energy spectrum (e.g., Pan et al. 2012; Fu et al. 2013b, 2019; Liu et al. 2017c). The non-adiabatic process, stemming from the interaction between electrons and waves around the DF (such as lower hybrid waves, magnetosonic waves, whistler-mode waves, etc.; e.g., Wei et al. 2007; Zhou et al. 2009; Khotyaintsev et al. 2011; Fu et al. 2012c, 2014a, 2014b; Hwang et al. 2014; Divin et al. 2015; Liu et al. 2017b), can violate the adiabaticity and affect the acceleration efficiency. These electron acceleration processes can efficiently transfer energies between particles and electromagnetic fields around the DF (e.g., Angelopoulos et al. 2013; Huang et al. 2015a; Fu et al. 2017; Yao et al. 2017; Liu et al. 2018a, 2018b, 2018c, 2019).

Recently, spacecraft observations (e.g., Fu et al. 2011; Turner et al. 2016; Liu et al. 2017b, 2017c) and numerical simulations (e.g., Ashour-Abdalla et al. 2011) have suggested that electron acceleration behind the DF may just occur in certain energy ranges. In particular, electron acceleration can happen only at energies higher than a threshold. Such a scenario is reminiscent of the electron acceleration process in the radiation belt (e.g., Summers et al. 2002), where such an energy threshold is referred to as an "anchor point." Here we borrow this terminology to describe the electron acceleration behind the DF. In the spacecraft measurements, this anchor point may significantly affect the electron energy spectrum behind the DF. Specifically, when the anchor point is low (Cluster 2006 September 3 event, Figures 1(a)–(f)), the electron energy spectrum exhibits a flux-decrease feature in the low-energy range, but a flux-increase feature in the high-energy range (see Figure 1(e)); when the anchor point is high (Cluster 2006 October 14 event, Figures 1(g)–(l)), the electron energy spectrum exhibits a flux-decrease feature in the full energy range from 0 to 26 keV (see Figure 1(k)). In this regard, understanding the anchor point is very important, particularly for revealing the electron dynamics behind the DF. However, so far, what determines this point and how it is formed remain unknown.

In this Letter we study for the first time the anchor point of electron acceleration inside the DFB (the strong-$B_z$ region during and after the front has passed in a certain time series, see

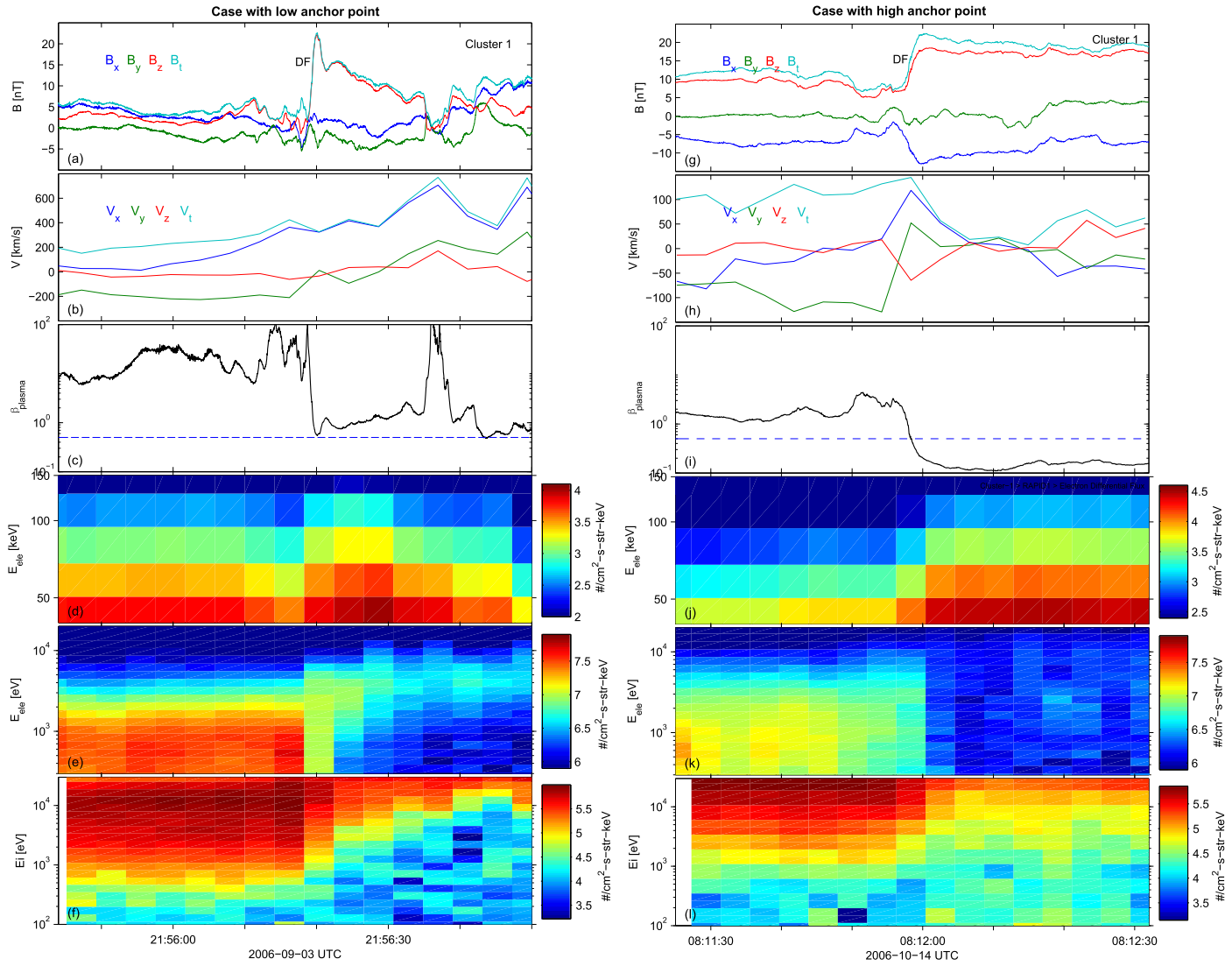


**Figure 1.** Electron acceleration with different anchor points during two DF crossings. (a), (g) the magnetic field; (b), (h) ion velocity; (c), (i) plasma beta with blue dashed line denoting the value of 0.5; (d)–(e), (j)–(k) electron energy spectrum; (f), (l) ion energy spectrum.

the detailed definition below) behind the DFs by considering a large amount of DF events collected by Cluster during 2001–2009. We investigate the anchor point's global distribution in the magnetotail, examine its relation with plasma properties around the DF, and discuss the role of waves in determining this anchor point. The key purpose of our study is to establish an empirical model for predicting electron acceleration behind a DF by monitoring ambient plasma sheet. This model is crucial for forecasting space weather as the accelerated electrons in the FPR will be further transported into the inner magnetosphere, providing source population for "relativistic electrons" in the radiation belt (e.g., Turner et al. 2016; Liu et al. 2017b). We show a case present an example of an anchor point in Section 2, establish an empirical model for the anchor point in Section 3, and finally present our conclusions in Section 4.

## 2. Case Study

Data from the Cluster mission, particularly from the Ion Spectrometry (CIS) experiment, the Fluxgate Magnetometer (FGM) experiment, the Research with Adaptive Particle Imaging Detectors (RAPID), the Plasma Electron And Current Experiment (PEACE), and the Spatio Temporal Analysis of Field Fluctuations (STAFF) instrument are used in this study. All the data are presented in the GSM coordinates unless stated otherwise.

We first present a case to illustrate how the anchor point is involved during electron acceleration behind the DF. The event of interest, observed by Cluster 1 on 2006 October 4 at $[-14.9, 3.88, -0.26]\,R_E$, is shown in Figure 2. As can be seen, before ~19:52:10 UT, C1 was located in the quiet plasma sheet. During this interval, the magnetic field strength was weak ($B_z \sim 1$ nT, Figure 2(a)), and the ion temperature and density were steady (Figures 2(e) and (f)). From 19:51:40 to 19:52:20 UT, the ion velocity $V_x$ gradually increased from 0 to 200 km s$^{-1}$ (Figure 2(b)), corresponding to the precursor flow ahead of the DF (e.g., Zhou et al. 2010; Wang et al. 2017). The DF structure was detected at ~19:52:23 UT, as indicated by the sharp increase of $B_z$ (from 1 to 19 nT, Figure 2(a)) and decrease of ion density (Figure 2(e)). Behind the DF, the DFB is identified as the strong-$B_z$ region ($B_z > 10$ nT, Figure 2(a))

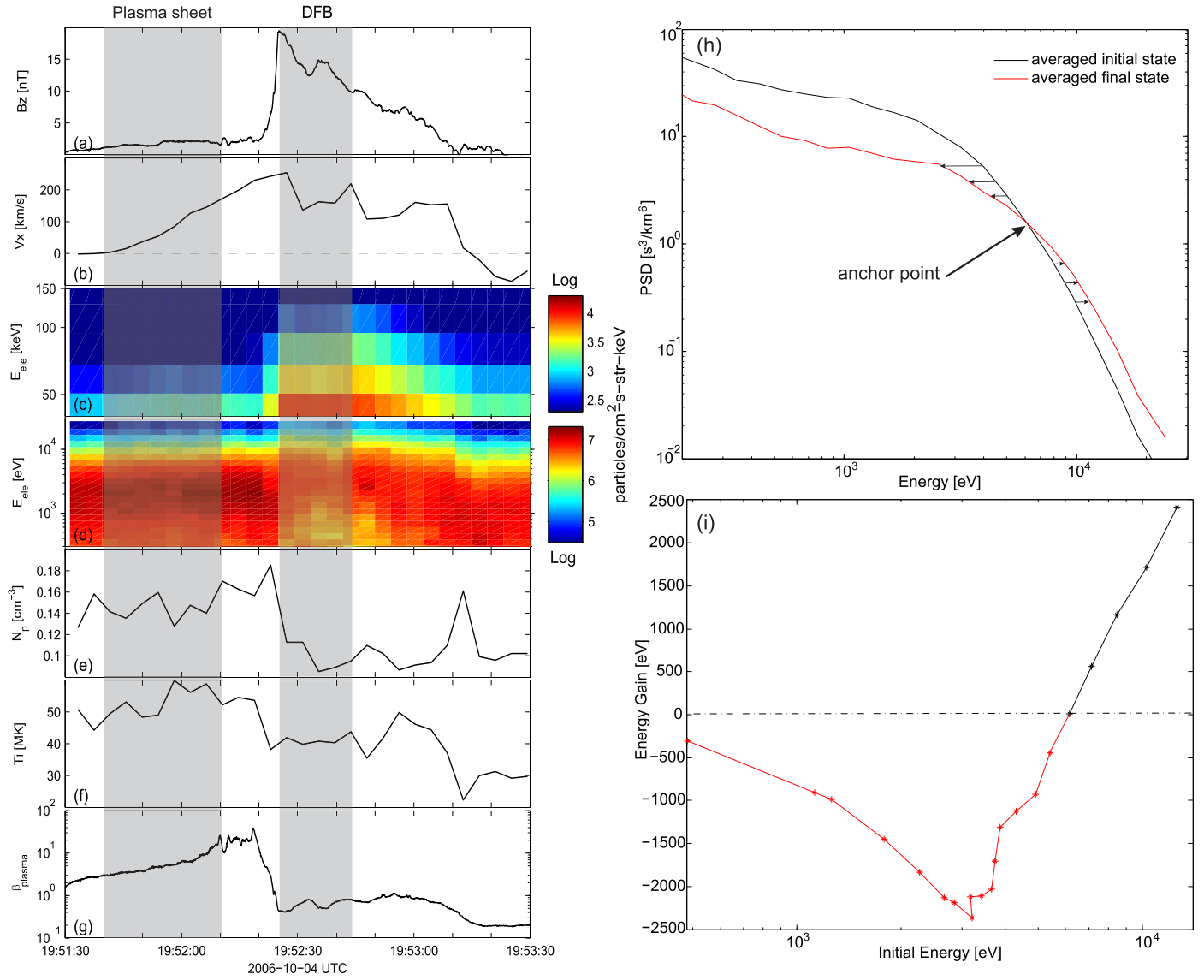


**Figure 2.** Cluster observations of electron acceleration behind a DF. (a) $B_z$ of the magnetic field; (b) $V_x$ of ion flow velocity; (c) and (d) electron spectrogram; (e) ion density; (f) ion temperature; (g) plasma beta; (h) averaged phase space density (PSD) evolution; (i) electron energy gain in the adiabatic regime after acceleration.

from 19:52:23 to 19:52:45 UT (e.g., Runov et al. 2015). Because the ion flow decreased inside the DFB, it may be referred to as a decaying DFB (Fu et al. 2011, 2012c).

Strong electron energization was observed inside the DFB, as shown in Figures 2(c) and (d). Electron spectrograms observed by the RAPID (Figure 2(c)) and PEACE instruments (Figure 2(d)) show consistent evolution during the DF crossing. Electron fluxes of different energy channels measured by the RAPID instrument simultaneously display dramatic enhancement inside the DFB (Figure 2(c)), indicating that electron acceleration inside the DFB is dispersionless. Nevertheless, electron fluxes at different energy channels measured by the PEACE instrument exhibit dispersive characteristics, with the increase of fluxes at >6 keV and the decrease of fluxes at <6 keV. Such a dispersive feature of electron fluxes has been reported previously in spacecraft observations (e.g., Deng et al. 2010; Khotyaintsev et al. 2011; Turner et al. 2016) and numerical simulations (e.g., Ashour-Abdalla et al. 2011; Gabrielse et al. 2012; Birn et al. 2014), which suggests that the electrons at different energies drift to the spacecraft from a variety of different locations, and is an indication of the anchor point during electron acceleration.

To investigate this point, we focus on the evolution of electron phase space density (PSD) in the energy range of the PEACE instrument. Similar to previous studies (e.g., Fu et al. 2011, 2013b; Runov et al. 2015; Turner et al. 2016; Liu et al. 2017b, 2017c; Xu et al. 2018b), we assume the pre-existing electrons (between 19:51:40 and 19:52:10 UT) as the "source population" (or averaged initial state). Note that in the Earth's magnetotail, electron energy distribution displays a global change due to $B_z$ variation (Artemyev et al. 2013); however, such change does not affect our analysis, which is mainly based on observations of DFB in the midtail ($X_{\rm GSM} < -14\,R_E$; see discussions below). Our assumption is reasonable because there is a close connection between plasma-sheet electrons and DFB electrons: plasma-sheet electrons can be accelerated inside the reconnection diffusion region and further accelerated inside the DFB; plasma-sheet electrons can enter into the FPR via cross-tail drift from the inner tail or reconnection entry from the distant tail (e.g., Birn et al. 2013, 2014); plasma sheet can

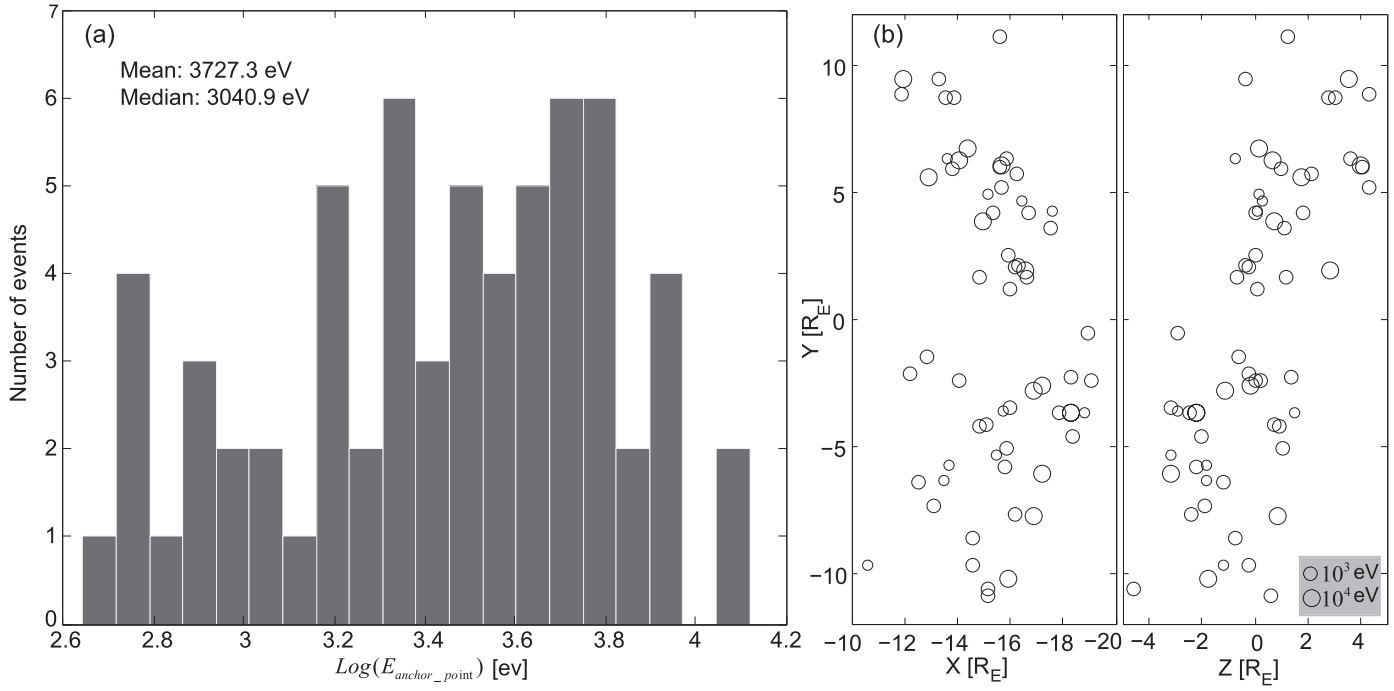


**Figure 3.** (a) Histogram of anchor point distribution. (b) Global distribution of anchor points in the dawn–dusk and north–south directions in the magnetotail. The size of the circle in Figure 3(b) denotes the value of the anchor point.

also exchange electrons with the DFB via instabilities (e.g., Liu et al. 2018c) and plasma vortex around the DF (e.g., Gabrielse et al. 2012); the close connection between plasma-sheet electrons and DFB electrons has been recently confirmed by a comprehensive statistical study (Runov et al. 2015) where the plasma-sheet electrons are found to be the "source" of DFB electrons. For comparison, we use the electron population inside the DFB as the "resultant population" (or averaged final state). As shown in Figure 2(h), we can clearly see that the PSD increases at >6.2 keV, but decreases at <6.2 keV. As in previous studies (Liu et al. 2017a, 2017c), we further analyze the energy gain during the electron acceleration process using the Liouville mapping. According to the Liouville theorem, the averaged initial state PSD and the averaged final state PSD are correlated by the following equation (e.g., Egedal et al. 2010; Liu et al. 2017a, 2017c):

$$F_{\rm initial}(E_{\rm initial}(E_{\rm final})) = F_{\rm final}(E_{\rm final}) \quad (1)$$

where $E_{\rm final}$ and $E_{\rm initial}$ are the electron energies before mapping and after mapping, respectively. The mapping results are shown in Figure 2(i). As can be seen, only at energies higher than 6.2 keV can the electron gain energy. This indicates that the anchor point of electron acceleration in this event is 6.2 keV. Note that in the non-adiabatic regime, a decrease of electron PSD at energies below this anchor point may arise from wave-particle interactions that are frequently reported near the DF.

## 3. Statistical Analyses

To date, what determines the anchor point and how it is formed remains unknown. To study this issue, we statistically analyze the electron acceleration behind DFs, by using the DF database collected by Cluster during 2001–2009 (during this period, Cluster preferred to stay in the south hemisphere and tailward region; its orbital coverage has been given by Fu et al. (2012b, see Figure 3)). For the DF database, we distinguish DF from single boundary crossing out of the central plasma sheet by using specific criteria, such as large plasma beta $\beta > 0.5$, large ion velocity $V_x > 150\ {\rm km\ s^{-1}}$, and large inclination angle of the magnetic field. The database that we used is the same as that in Fu et al. (2012b), where these criteria have been clarified in detail. We have also examined all events in the database and found no signature of lobe crossing. With the DF database, we first select the DF events with significant electron acceleration. Specifically, we consider the following two criteria: (1) the fluxes of high-energy electrons ($E > 20$ keV) are significantly high ($F > 500/{\rm cm^2\ s\ sr\ keV}$); (2) these fluxes have a clear enhancement behind the DF ($\delta F > 100/{\rm cm^2\ s\ sr\ keV}$). There are in total 182 cases being satisfied with these criteria in the database of Fu et al. (2012b). Among these 182 cases, 64 cases include clear anchor points during the acceleration behind DFs. Figure 3 shows the distribution of these anchor points. We see that the distributions of anchor points basically cover the energy space, indicating that the obtained database is suitable for investigating the properties of anchor points. In the histogram (Figure 3(a)), we can see that the anchor points vary over a broad range, from 440 eV to 13 keV, with a mean value of 3727.3 eV and a median value of 3040.9 eV. This value is comparable to the electron thermal energy in the plasma sheet (e.g., Runov et al. 2015).

Figure 3(b) shows the spatial distribution of these anchor points in the magnetotail. We find no clear asymmetry of anchor point distribution in the north–south and dawn–dusk directions, suggesting that anchor points are not affected by the dusk–dawn asymmetry of the magnetotail plasma. Also, we find no clear evolution of the anchor point when DFs propagate toward the Earth, meaning that the global change of the magnetotail magnetic field associated with the DF propagation does not affect the anchor point either. This further confirms

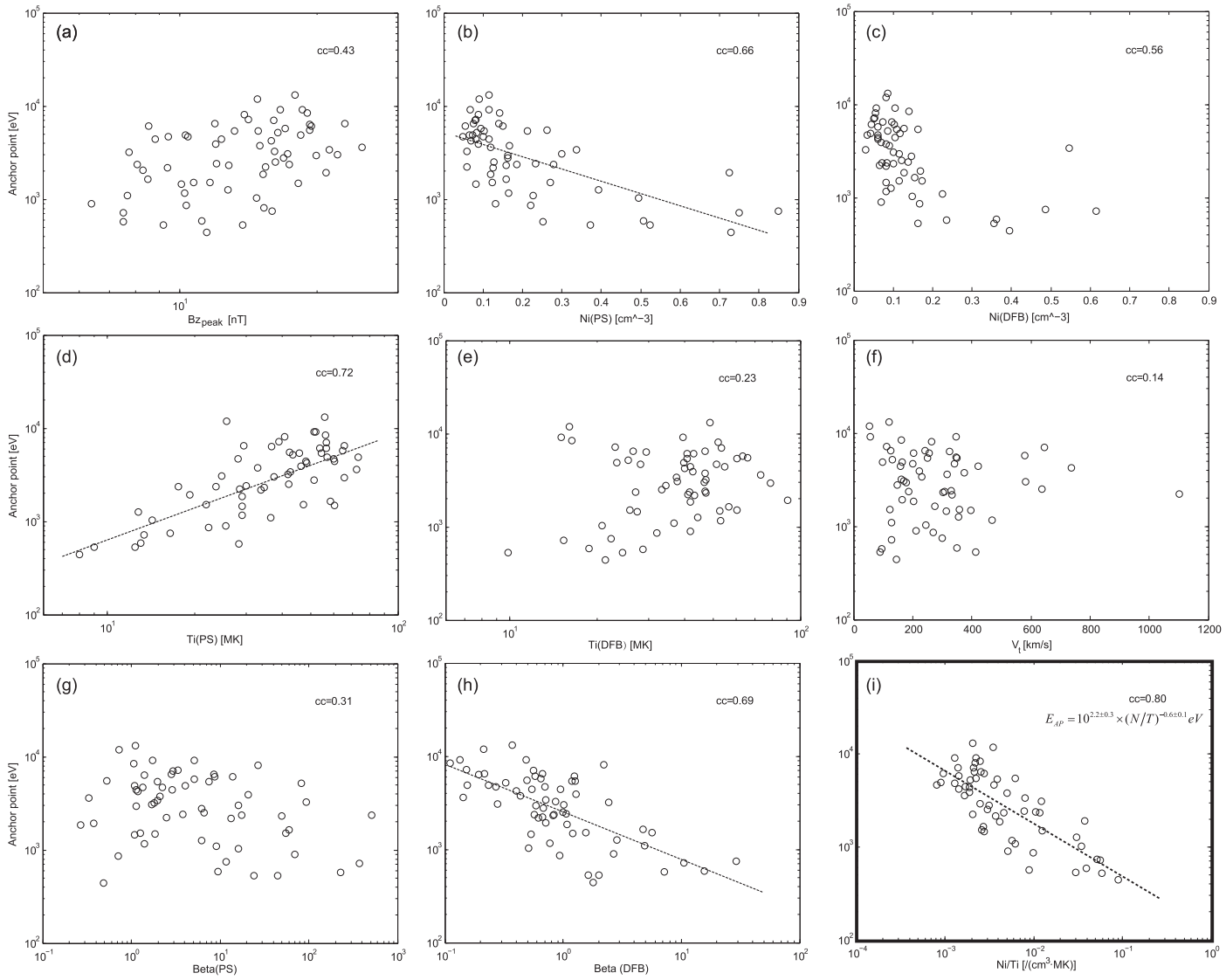


**Figure 4.** Correlation analysis between anchor point and local plasma properties including (a) the peak of $B_z$ measured inside the DFB; (b)–(c) ion density inside the plasma sheet and the DFB; (d)–(e) ion temperature inside the plasma sheet and the DFB; (f) absolute value of ion velocity; (g)–(h) plasma beta inside the plasma sheet and the DFB; (i) a fitting function of the correlation between the anchor point and plasma-sheet density and temperature by maximizing correlation coefficient.

that a global change of electron energy distribution in the magnetotail does not affect our above analysis. Therefore, the electron anchor point is not attributed to the global properties of magnetotail plasma, but may be locally determined by plasma population around the DFs.

To investigate how plasma properties affect the anchor point during acceleration behind DFs, we conduct a correlation analysis between the anchor point and the plasma properties in the undisturbed plasma sheet and in the DFB. We obtain the plasma-sheet properties, which are used as the properties of the "source population" (or averaged initial state), by averaging plasma parameters in a 30 s duration before the $B_z$ peak (from $t_{DF}$-40 to $t_{DF}$-10 s, $t_{DF}$ is the time when $B_z$ reaches its peak), and obtain the plasma parameters inside the DFB, which are used as the properties of the "resultant population" (or averaged final state), by averaging plasma parameters in a 10 s duration behind the $B_z$ peak (from $t_{DF}$ to $t_{DF}+10$ s). We particularly focus on the ion temperature, density, plasma beta, $B_z$ peak (the peak of $B_z$ measured inside the DFB), and flow velocity in these two regions. We do not consider the electron density and temperature, because these parameters measured by C1 have a very low resolution (Johnstone et al. 1997). However, the ion–electron temperature ratio in the plasma sheet is roughly steady, with an averaged value of ∼6.0 (Grigorenko et al. 2016).

The correlation analysis results are shown in Figure 4. We see that the anchor point is not correlated with the $B_z$ peak (Figure 4(a)), indicating that betatron acceleration, typically occurring at the DF (e.g., Fu et al. 2011, 2013b; Liu et al. 2017a, 2017b, 2017c), does not affect the anchor point. Interestingly, we find that the anchor point is well correlated with the plasma-sheet density and temperature (Figures 4(b) and (d)), with the correlation coefficients of ∼0.7. In contrast, it shows no clear correlation with plasma density and temperature inside the DFB (Figures 4(c) and (e)). This suggests that the anchor point is related to the "source population" but not related to the "resultant population." Moreover, we see that the anchor point is not clearly correlated with the ion flow velocity (Figure 4(f)), indicating that anchor point is not affected by the high-speed jets associated with the DF. Also, we find that anchor point is not correlated with plasma beta inside the

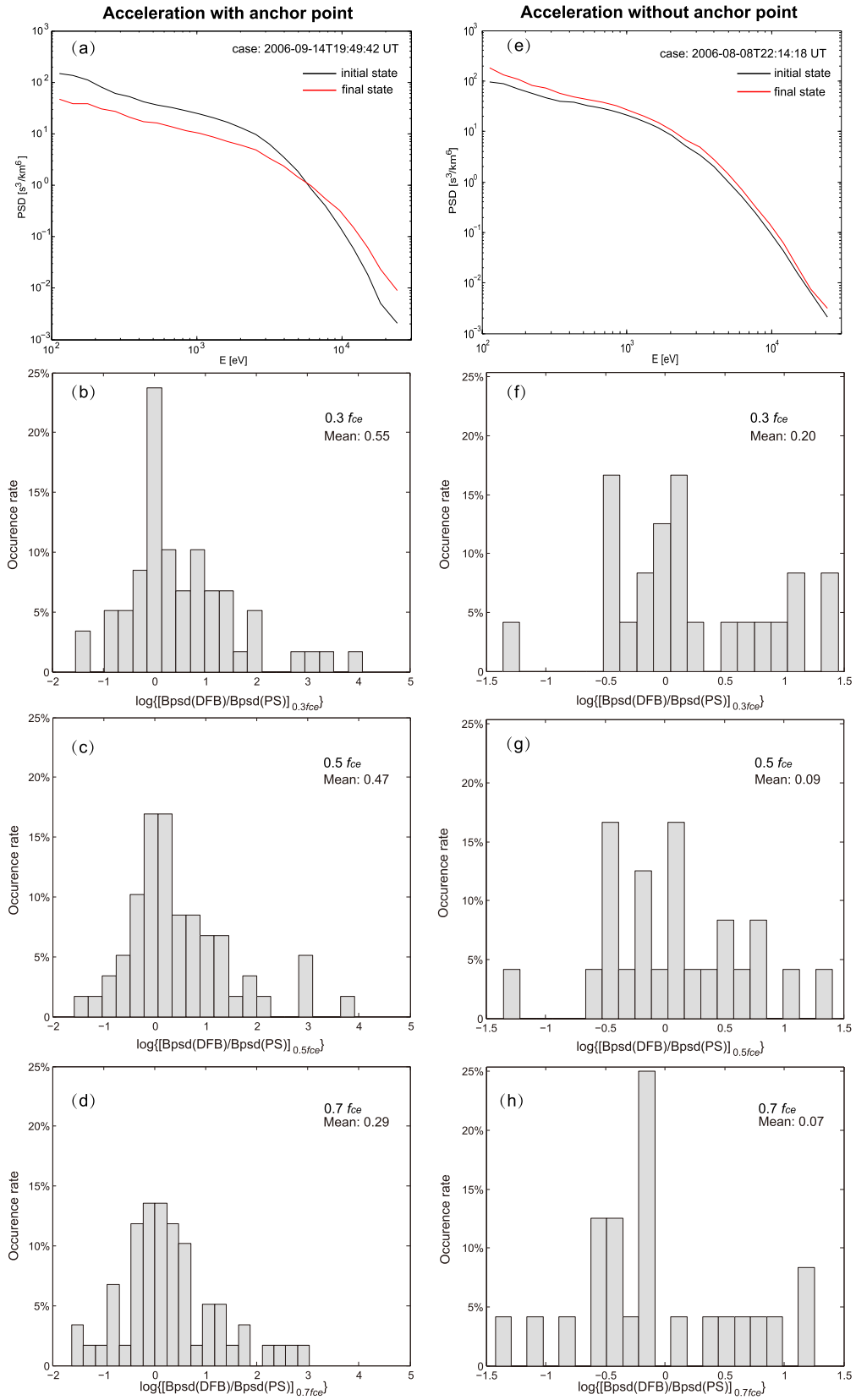


**Figure 5.** Comparison of wave intensity at whistler frequency range between acceleration events with anchor points vs. acceleration events without anchor points. (a) PSD evolution showing acceleration with anchor points, where the black and red lines represent the initial and final states, respectively; (b)–(d) distribution of the intensification of waves in event database with anchor point at frequencies of 0.3 $f_{ce}$, 0.5 $f_{ce}$, and 0.7 $f_{ce}$, respectively; (e) PSD evolution showing acceleration without anchor points, where the black and red lines representing the initial and final states, respectively; (b)–(d) distribution of the intensification of waves in event database without anchor point at frequencies of 0.3 $f_{ce}$, 0.5 $f_{ce}$, and 0.7 $f_{ce}$, respectively.

plasma sheet (Figure 4(g)), which is consistent with the absence of asymmetry of anchor point distribution in the north–south directions in the magnetotail. However, we notice that the anchor point is negatively correlated with plasma beta inside the DFB, with the correlation coefficients of ∼0.69, suggesting that anchor point is higher in low-beta DFB.

Based on the good correlation between the anchor point and the plasma-sheet density and temperature, we establish a model for the anchor point, in order to predict the electron acceleration processes inside the DFBs behind DFs. First we examine correlation between the anchor point and the parameter $N^a/T$ ($a$ is the power-law index of the number density); We find that it gives the maximum correlation coefficient when the index $a$ is equal to 1. Then we derive the model by fitting their correlation as

$$E_{\rm AP} = 10^{2.2\pm0.3} \times (N/T)^{-0.6\pm0.1}\ {\rm eV} \quad (2)$$

with a maximum correlation coefficient of 0.8 (see Figure 4(i)). Here the plasma-sheet density $N$ is normalized to 1 $\rm cm^{-3}$, and the plasma-sheet temperature $T$ is normalized to 1 MK. This function, linking the anchor point with the plasma properties inside the plasma sheet, has an important implication for the electron acceleration behind DFs and thus can be used to forecast the anchor point. Note that the anchor point is proportional to the temperature of ambient plasmas but inverse-proportional to the density, indicating that the anchor point is higher in hot tenuous plasmas than in cold dense plasmas. It is worthwhile to note that the anchor point also exists in electron acceleration regions elsewhere in space, such as reconnection diffusion region and collisionless shocks.

Results of the correlation analysis may implicate the underlying physics of anchor points. We find that this point is well correlated with the plasma-sheet temperature and density, and the plasma beta inside the DFB, but not with the $B_z$ peak, flow velocity, and plasma density and temperature inside the FPR. Correlation between the anchor point and the plasma-sheet density and temperature suggests that the anchor point is locally affected by particle characteristics ahead of the DF; in other words, the electron anchor point is directly related to the source population. As a clear correlation between the anchor point and the $B_z$ peak, flow velocity, and density and temperature inside DFB is not found, the formation of the anchor point behind DFs cannot be explained using the adiabatic effect (e.g., Fu et al. 2011; Birn et al. 2014; Runov et al. 2015; Liu et al. 2017b). In fact, adiabatic effects do not change the power-law index in the energy spectrum (e.g., Pan et al. 2012; Fu et al. 2013b; Liu et al. 2017c) and thus theoretically cannot lead to the formation of anchor point. This indicates that non-adiabatic effect (or wave-particle interactions) should be involved for forming the anchor point during DF-associated acceleration (e.g., Turner et al. 2016). Because waves from low hybrid frequency to electron cyclotron frequency are very common around the DF, interaction between these waves and electrons may play a crucial role in the formation of an anchor point.

To investigate the role of waves in the formation of an anchor point, a comparison analysis between the events with an anchor point and the events without an anchor point is necessary. We conduct such analysis by utilizing the DF database, with a particular focus on the waves in the frequency range of whistlers, because these waves can efficiently mediate the energy transfer between low-energy electrons and high-energy electrons (e.g., Shklyar 2017), which can lead to the formation of an anchor point, and their intensity can be easily obtained from the spacecraft data. We quantify the intensification of these waves in the events both with and without anchor points by examining the PSD of magnetic field at $0.3\,f_{ce}$, $0.5\,f_{ce}$, and $0.7\ f_{ce}$ ($f_{ce}$ is the electron cyclotron frequency). The comparison results are shown in Figure 5. Specifically, Figure 5(a) displays the evolution of the electron PSD during acceleration with anchor point, and Figures 5(b)–(d) show the intensification of waves in the events with an anchor point. By contrast, Figure 5(e) presents the evolution of the electron PSD during acceleration without an anchor point, and Figures 5(f)–(h) show the intensification of waves in the events without an anchor point. We find that, at $0.3\ f_{ce}$, $0.5\,f_{ce}$, and $0.7\ f_{ce}$, the mean values of the wave power enhancement are generally large in the events with an anchor point (Figures 5(b)–(d)) but small in the events without an anchor point (Figures 5(f)–(h)). This suggests that wave-particle interactions may play a crucial role in the formation of an anchor point during acceleration behind DFs. A theoretical explanation possibly accounting for the formation of anchor points is that resonant wave-particle interaction represents a conduit for the energy transfer between low-energy electrons and high-energy electrons: the low-energy electrons (the thermal electrons) give their energy to the whistler waves, and then the wave energy is absorbed by the high-energy electrons (e.g., Shklyar 2017). We will further study the viability of this mechanism and investigate the role of other types of waves, such as lower hybrid drift waves and magnetosonic waves, by using the high-resolution measurements of particles and fields from the MMS mission in the future.

## 4. Conclusions

In conclusion, we investigate the formation of anchor points and the relation between these points and the plasma properties for the first time, by considering a large amount of DF events measured by Cluster during 2001–2009. We notice that such points appear primarily in the DF events associated with strong waves, suggesting that they are formed due to wave-particle interactions near DFs. Through correlation analysis, we find a good correlation between anchor points and plasma-sheet density and temperature. Based on this correlation, we quantitatively establish a model for the anchor point during DF-associated electron acceleration, $E_{\rm AP} = 10^{2.2\pm0.3} \times (N/T)^{-0.6\pm0.1}$ eV, where $N$ and $T$ are the plasma-sheet density and temperature, respectively. With this model, we can predict the electron acceleration features behind DFs, by monitoring plasma properties in the plasma sheet. These findings are crucial, in particular, for understanding the electron dynamics around DFs.

We thank Cluster Science Archive (http://www.cosmos.esa.int/web/csa) for providing the data for this study. This work was supported by NSFC grants 41574153, 41431071, and the ISSI travel grant for team "MMS and Cluster Observations of Magnetic Reconnection."

## ORCID iDs

C. M. Liu https://orcid.org/0000-0002-9705-5387
H. S. Fu https://orcid.org/0000-0002-4701-7219

## References


Angelopoulos, V., Runov, A., Zhou, X.-Z., et al. 2013, Sci, 341, 1478
Artemyev, A. V., Petrukovich, A. A., Nakamura, R., & Zelenyi, L. M. 2013, AnGeo, 31, 1109
Ashour-Abdalla, M., El-Alaoui, M., Goldstein, M. L., et al. 2011, NatPh, 7, 360
Birn, J., Hesse, M., Nakamura, R., & Zaharia, S. 2013, JGRA, 118, 1960
Birn, J., Runov, A., & Hesse, M. 2014, JGRA, 119, 3604
Cao, J. B., Duan, J. T., Du, A. M., et al. 2008, JGRA, 113, A07S15
Cao, J. B., Ma, Y. D., Parks, G., et al. 2006, JGR, 111, A04206
Cao, J. B., Ma, Y. D., Parks, G., et al. 2013, JGRA, 118, 313
Deng, X. H., Ashour-Abdalla, M., Zhou, M., et al. 2010, JGR, 115, A09225
Divin, A., Khotyaintsev, Y. V., Vaivads, A., et al. 2015, JGRA, 120, 2675
Duan, A. Y., Cao, J. B., Dunlop, M., & Wang, Z. Q. 2014, JGRA, 119, 8902
Egedal, J., Lê, A., Zhu, Y., et al. 2010, GeoRL, 37, L10102
Fu, H. S., Cao, J. B., Cully, C. M., et al. 2014a, JGRA, 119, 9089
Fu, H. S., Cao, J. B., Khotyaintsev, Y. V., et al. 2013a, GeoRL, 40, 6023
Fu, H. S., Cao, J. B., Zhima, Z., et al. 2014b, GeoRL, 41, 7419
Fu, H. S., Khotyaintsev, Y. V., André, M., Vaivads, A., et al. 2011, GeoRL, 38, L16104
Fu, H. S., Khotyaintsev, Y. V., Vaivads, A., et al. 2012a, GeoRL, 39, L06105
Fu, H. S., Khotyaintsev, Y. V., Vaivads, A., et al. 2012b, GeoRL, 39, L10101
Fu, H. S., Khotyaintsev, Y. V., Vaivads, A., et al. 2012c, JGR, 117, A12221
Fu, H. S., Khotyaintsev, Y. V., Vaivads, A., et al. 2013b, NatPh, 9, 426
Fu, H. S., Vaivads, A., Khotyaintsev, Y. V., et al. 2017, GeoRL, 43, 37
Fu, H. S., Xu, Y., Vaivads, V., & Khotyaintsev, Y. V. 2019, ApJL, 870, L22
Gabrielse, C., Angelopoulos, V., Runov, A., & Turner, D. L. 2012, JGR, 117, A10213
Grigorenko, E. E., Kronberg, E. A., Daly, P. W., et al. 2016, JGRA, 121, 9985
Huang, C., Wu, M., Lu, Q., Wang, R., & Wang, S. 2015a, JGRA, 120, 1759
Huang, S. Y., Fu, H. S., Yuan, Z. G., et al. 2015b, JGRA, 120, 4496
Huang, S. Y., Zhou, M., Deng, X. H., et al. 2012, AnGeo, 30, 97
Hwang, K.-J., Goldstein, M. L., Vinas, A. F., et al. 2014, JGRA, 119, 2484
Johnstone, A. D., Alsop, C., Burge, S., et al. 1997, SSRv, 79, 351
Khotyaintsev, Y. V., Cully, C. M., Vaivads, A., et al. 2011, PhRvL, 106, 165001
Liu, C. M., Chen, Z. Z., Wang, Z., & Liu, Y. Y. 2019, ApJ, 871, 209
Liu, C. M., Fu, H. S., Cao, J. B., et al. 2017a, GeoRL, 44, 10116
Liu, C. M., Fu, H. S., Cao, D., et al. 2018a, ApJ, 860, 128
Liu, C. M., Fu, H. S., Vaivads, A., et al. 2018b, GeoRL, 45, 556
Liu, C. M., Fu, H. S., Xu, Y., et al. 2017b, JGRA, 122, 594
Liu, C. M., Fu, H. S., Xu, Y., et al. 2017c, GeoRL, 44, 6492
Liu, C. M., Fu, H. S., Xu, Y., et al. 2018c, GeoRL, 45, 4628
Liu, C. M., Liu, Y. Y., Xu, Y., et al. 2018d, ApJ, 866, 93
Liu, J., Angelopoulos, V., Runov, A., & Zhou, X.-Z. 2013, JGRA, 118, 2000
Lu, S., Angelopoulos, V., & Fu, H. S. 2016, JGRA, 121, 9483
Nakamura, R., Baumjohann, M., Klecker, B., et al. 2002, GeoRL, 29, 1942
Pan, Q., Ashour-Abdalla, M., El-Alaoui, M., et al. 2012, JGRA, 117, A12224
Pritchett, P. L., & Runov, A. 2017, JGRA, 122, 3183
Runov, A., Angelopoulos, V., Gabrielse, C., et al. 2015, JGRA, 120, 4369
Runov, A., Angelopoulos, V., Sitnov, M. I., et al. 2009, GeoRL, 36, L14106
Sergeev, V., Angelopoulos, V., Apatenkov, S., et al. 2009, GeoRL, 36, L21105
Shklyar, D. R. 2017, JGRA, 122, 640
Sitnov, M. I., Swisdak, M., & Divin, A. 2009, JGR, 114, A04202
Summers, D., Ma, C., Meredith, N. P., et al. 2002, GeoRL, 29, 2174
Turner, D. L., Fennell, J. F., Blake, J. B., et al. 2016, GeoRL, 43, 7785
Wang, J., Cao, J. B., Fu, H. S., et al. 2017, JGRA, 122, 185
Wei, X. H., Cao, J. B., Zhou, G. C., et al. 2007, JGR, 112, A10225
Wu, M. Y., Lu, Q. M., Volwerk, M., et al. 2013, JGRA, 118, 4804
Xu, Y., Fu, H. S., Hwang, K. J., & Liu, C. M. 2018a, PhPl, 25, 072123
Xu, Y., Fu, H. S., Liu, C. M., & Wang, T. Y. 2018b, ApJ, 853, 11
Yang, J., Cao, J. B., Fu, H. S., et al. 2017, JGRA, 122, 4299
Yao, Z. H., Liu, J., Owen, C. J., et al. 2015, AnGeo, 33, 1301
Yao, Z. H., Rae, I. J., Guo, R. L., et al. 2017, JGRA, 122, 4335
Zhou, M., Ashour-Abdalla, M., Deng, X. H., et al. 2009, GeoRL, 36, L20107
Zhou, M., Deng, X. H., Ashour-Abdalla, M., et al. 2013, JGRA, 118, 674
Zhou, X. Z., Angelopoulos, V., Sergeev, V. A., & Runov, A. 2010, JGR, 115, A00I03